Inorganic Chemistry

pubs.acs.org/IC

Communication

Ionothermal Synthesis of an Antimonomolybdate Cluster, $[Sb_8Mo^{VI}_{13}Mo^{V}_5O_{66}]^{5-}$, and Its Catalytic Behavior to the Reduction of Nitrobenzene

Shu-Kui Shi, Xin Li, Hui-li Guo, Yan-hua Fan, Hai-yan Li, Dong-Bin Dang,* and Yan Bai*

Cite This: https://dx.doi.org/10.1021/acs.inorgchem.0c00825

ABSTRACT: The largest antimonomolybdate monomer, $[Sb_8Mo^{VI}_{13}Mo^{V}_5O_{66}]^{5-}$ (**1-Sb_8Mo_{18}**), has been isolated and displays a new breakthrough of polyoxometalates (POMs) with an ionothermal synthesis strategy. **1-Sb_8Mo_{18}** features the first hexanuclear sandwich-type polymolybdate (POMo) with an unexpected metal ring $\{Sb_6O_{12}\}$ to make its debut in Sb clusters. Furthermore, **1-Sb_8Mo_{18}** exhibits a prominent catalytic activity for reducing nitrobenzene to aniline with excellent sustainability.

Polyoxometalates (POMs) are discrete polyatomic ion clusters formed by O and early-transition-metal atoms in their high oxidation states.[1−3] As a large and rapidly growing series of inorganic compounds, POMs have attracted great attention and been widely studied because of their unmatched range of structural features, sizes, and chemical and physical properties, which applies to diverse areas such as catalysis, medicine, functional materials, etc.[4−7] As an important branch of POMs, lacunary POMs have a well-defined structure and high reactive vacant sites that provide a lot of decent opportunities to combine with organic ligands or metal species.[8−10] Therefore, lacunary POMs are considered to be remarkable multidentate building blocks to construct POM-based polynuclear clusters. According to this approach, a great number of attractive POMs based on lacunary polyoxotungstates (POTs) have been reported, but for lacunary polymolybdates (POMos), there are only a few examples. First, the separation of lacunary POMos is very difficult in the aqueous solution because of their quite intricate equilibria presence. Second, their extreme mutability in water can easily lead to saturation or decomposition by a slight change of the environment.[11−13] Very recently, Suzuki and co-workers utilized organic media to hold the stability of lacunary POMo $[A\text{-}\alpha\text{-}PMo_9O_{34}]^{9-}$ and produce three novel POM−organic structures, $[A\text{-}\alpha\text{-}PMo_9O_{31}(py)_3]^{3-}$, $[(A\text{-}\alpha\text{-}PMo_9O_{31})_2(bpy)_3]^{6-}$, and $[(PMo_9O_{31})_4(tpyp)_2]^{12-}$ (py = pyridine, bpy = 4,4′-bipyridine, and tpyp = 5,10,15,20-tetra-4-pyridylporphyrin).[14] This finding strongly confirms that introducing a nonaqueous solvent to the reaction system would be a facile strategy to stabilize lacunary POMos.

Ionic liquids (ILs) have been regarded as an ideal alternative to the traditional molecular water or volatile organic solvents in the process of synthesis because of their ion's nature and unique advantages such as negligible vapor pressure and high chemical and thermal stability.[15−19] The application of ILs in inorganic synthesis, especially ionothermal synthesis, has been rapidly developed since ILs were used to synthesize zeolitic solids by Morris in 2004,[20,21] In recent years, such an ionothermal method has been extended to the preparation of new POMs with novel structure, and some exciting results have been reported, for example, the high-nuclearity Fe-substituted POM $[WFe_9O_{13}(SiW_9O_{34})_3]^{23-}$, a high-nuclearity Ag_{70} shell encapsulating two lacunary $[PW_9O_{34}]^{9-}$ cores $[Ag_{70}(PW_9O_{34})_2(^tBuC{\equiv}C)_{44}(H_2O)_2]^{8+}$, and the quantum-spin liquid candidate $[V_7O_6F_{18}]^{3-}$.[22−24]

Herein, using the ionothermal synthesis strategy, we successfully prepare an unprecedented antimonomolybdate structure, $[EMIm]_5[Sb_8Mo^{VI}_{13}Mo^{V}_5O_{66}]$ (**1-Sb_8Mo_{18}**), with the highest Sb/Mo ratio. The structure also represents a breakthrough of polynuclear clusters based on lacunary POMos, for there are only mono-, di-, and tetranuclear-substituted sandwich-type POMo structures that have been reported before (summarized in Table S2). It is worth mentioning that the ring-shaped substitute unit $[Sb_6O_{12}]$ also has not been observed in Sb-containing compounds to the best of our knowledge. It is necessary to emphasize that the self-assembly process is very sensitive to the solvent environment. The pure IL environment could give the only product of **1-Sb_8Mo_{18}**, while the existence of water in the system would result in the generation of the other two products of $[EMIm]_4[SiMo_{12}Sb_2O_{40}]$ (**2-$SiMo_{12}Sb_2$**) and $K[EMIm]_3[\beta\text{-}Mo_8O_{26}]$ (**3-Mo_8**), respectively (Experimental Section).

A detailed crystallographic analysis reveals that the anion is constituted by two trivacant Keggin $\{B\text{-}\alpha\text{-}SbMo_9O_{33}\}$ units and a ringlike $[Sb_6O_{12}]^{6-}$ cluster (Figure 1a), which is isostructural with the stannotungstate cluster $[Sn_8W_{18}O_{66}]^{8-}$.[25] The trivacant lacunary $\{B\text{-}\alpha\text{-}SbMo_9O_{33}\}$ unit is a derivative of the Keggin structure by the removal of three edge-sharing MoO_6 octahedra. In each of the $\{B\text{-}\alpha\text{-}$

Received: March 20, 2020

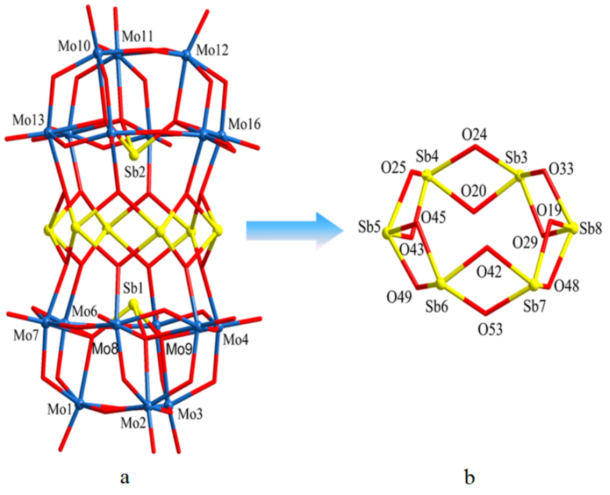

Figure 1. (a) Ball-and-stick representation of **1a** (right) and (b) the top view of the ring unit of $[Sb_6O_{12}]^{6-}$ (left). Average distances: 1.67(4) Å for Mo$=$O$_t$ (terminal oxygen), 1.92(3) Å for Mo$-\mu_2$-O (doubly oxygen), 2.09(5) Å for Mo$-\mu_3$-O (triply oxygen), and 2.28 Å for Mo$-\mu_4$-O (quadruply oxygen). Average Sb$-$O distances: 1.98(2) and 2.09(2) Å for $\{SbO_3\}$ and $\{SbO_4\}$, respectively.

$SbMo_9O_{33}\}$ hemispherical units, a crystallographically independent Sb atom (Sb1 or Sb2) is centered in it and coordinated by three O atoms to form the $\{SbO_3\}$ unit with a distorted pyramidal geometry, which is centered in a trivacant lacunary Keggin hemispherical unit and formed a $\{B\text{-}\alpha\text{-}SbMo_9O_{33}\}$ unit. So, the bare lone electron pair of the Sb atom point to the opposite position of the hemispherical unit and effectively restrict the extra octahedron MoO_6 to join into the lacunary unit. As far as we know, this is the third case about Sb-centered POMo, which is much rarer compared with that of the common species POT.[26−29] Two $\{SbMo_9O_{33}\}$ units, spinning approximately 60°, hold together in a face-to-face mode by the bridge connection of six crystallographically independent Sb atoms (from Sb3 to Sb8) to form the largest antimonomolybdate cluster $[Sb_8Mo_{18}O_{66}]^{5-}$ (**1a**) up to now. For the six Sb atoms, they connect each other one by one by the μ_3-O bridges to result in a ringlike $[Sb_6O_{12}]^{6-}$ unit (Figure 1b), which has not been reported before in the Sb-containing compounds. The distances of Mo$-$O and Sb$-$O are all located in the range of those found in other related POMs.[30−33] It is interesting to note that the six Sb atoms almost lie in a plane with a very small mean deviation of 0.03(5) Å, and the adjacent Sb⋯Sb distance and Sb⋯Sb⋯Sb angle are about 3.40(3) Å and 120°, respectively. Further analysis shows that [EMIm] cations are very important for enhancing the stability of the structure because they not only balance the charge of **1a** as counterions but also form numerous C$-$H⋯O hydrogen bonds with O atoms from anion clusters (Table S6).

A total of five $[EMIm]^+$ counterions contained in one **1-Sb$_8$Mo$_{18}$** unit suggest that the charge number of the **1a** anion would be 5−, which is confirmed by the results of charge conservation, bond-valence-sum calculation,[34] and X-ray photoelectron spectroscopy (XPS) measurement. As shown in Table S7, the bond valences of the Mo atoms are less than the value of Mo^{VI} except those of Mo3, Mo11, Mo12, and Mo16. The average value of 5.81 indicates that there are delocalized electrons located in those atoms. The oxidation states and chemometry of Mo atoms can be confirmed by the XPS data in the binding energy regions of Mo 3d. As shown in Figure S13, the peaks of Mo 3d observed at 232.6 and 235.8 eV and 231.8 and 234.9 eV are attributed to those of the Mo oxidation states for Mo^{VI} and Mo^{V}, respectively.[35,36] The ratio of Mo^{V}/Mo^{VI} directly obtained from the peak area is approximately 5:13 (Table S8), drawing a conclusion that there are 5 Mo^{V} and 13 Mo^{VI} atoms in the structure. Furthermore, the status of the delocalized electrons in **1a** has also been studied by the solid-state magnetic measurements. As shown in Figure S12, the effective magnetic moment of 1.75 μ_B for **1-Sb$_8$Mo$_{18}$** at room temperature is close enough for one spin-only Mo^{V} ion (1.73 μ_B), indicating that only one of the delocalized electrons is unpaired in the structure, while the other four electrons are paired. Such a magnetic behavior has been observed in other reduced POMs with an odd number of Mo^{V} atoms.[37−39]

The direct reduction of aromatic nitro compounds is one of the principal methods to obtain aromatic amines, and much effort has been devoted to developing efficient catalysts with cost-effectiveness for the reduction.[40−44] Reductions catalyzed by Lewis acid/base and ILs have been proven in previous works.[45−47] Very recently, Xu's group employed mixed-valence POMo as the catalyst to reduce the aromatic nitro compound and receive an unexpected result of high catalytic performance.[29,48,49] In view of the structure made up of a Lewis base anion of a mixed-valence antimonomolybdate cluster and IL cations of EMIm, an excellent catalytic activity to the reduction should be anticipated for **1-Sb$_8$Mo$_{18}$**.

The experiments of nitrobenzene reduction were employed with a 1:5 mole ratio of $ArNO_2$ and $N_2H_4{\cdot}H_2O$ in C_2H_5OH at 80 °C in a heterogeneous manner. After 2 h, almost 100% conversion of nitrobenzene to aniline was observed when 0.17 mol % **1-Sb$_8$Mo$_{18}$** was loaded as the catalyst (Table S10). In the blank experiments in which the catalyst **1-Sb$_8$Mo$_{18}$** or hydrazine was absent, almost no aniline or other intermediates were detected. In addition, termination of the reduction after moving out the catalyst at 40 min confirms a heterogeneous catalytic behavior of **1-Sb$_8$Mo$_{18}$** (Figure S15). The optimum catalytic condition was systematically researched by the catalyst-dependent catalytic activity and solvent-dependent catalytic performance (Table S12). The results show that the optimum catalytic condition would be regarded as a catalyst loading of 0.17 mol % in an alcohol solution. To the best of our knowledge, this catalyst loading is lower than most of the nitrobenzene reductions, which use $N_2H_4{\cdot}H_2O$ as the hydrogen source (Table S9), showing the cost-effectiveness of such a catalyst. Furthermore, various functionalized nitroarenes, such as chloro-, bromo-, and iodo-substituted nitrobenzenes, 4-nitrotoluene, and 2-nitrofluorene, were used to explore the general applicability of the catalyst **1-Sb$_8$Mo$_{18}$**. As shown in Table S11, the excellent isolated yields of anticipated anilines indicate that **1-Sb$_8$Mo$_{18}$** is a promising catalyst for nitrobenzene reduction.

As is known, intermediates always are used to analyze the mechanism of the catalytic reaction. The kinetic curves of the substances depicted in Figure 2 show that the intermediates of azoxybenzene and azobenzene can be detected after 20 min of reaction. Their concentrations were both slowly increased to a maximum at about 60 min and then faded away in the final product decrease along the prolonged reaction time. There are two pathways for the reduction of nitroarenes: direct and indirect routes (Scheme S1).[50−52] The detection of azoxybenzene and azobenzene suggests that an indirect route is adopted in the process. To verify the process, the reduction

https://dx.doi.org/10.1021/acs.inorgchem.0c00825

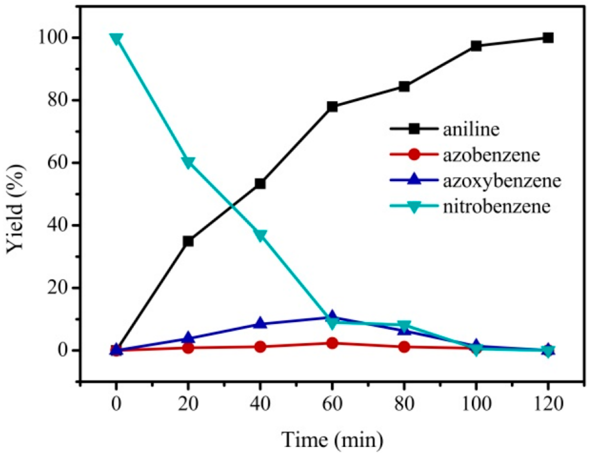

Figure 2. Kinetic curves for the reduction of $ArNO_2$ to aniline under 80 °C, catalyst **1-Sb_8Mo_{18}** (7.5 mg, 0.17 mol %), and N_2 atm.

experiments starting from azobenzene and *N*-phneylhydroxylamine under the same conditions were carried out. As shown in Table S11, the yields of 4-aminobenzene are about 99% for the former and 13% for the latter. A good conversion of azobenzene (95%) was observed only when the catalyst loading was increased to 1.7 mol %, indicating that it is not dominated by such an indirect route. These results suggested that both the direct and indirect routes should exist in the reduction process and the direct route might be the major one.[53,54]

In order to further explore the catalytic behavior of **1-Sb_8Mo_{18}**, comparative experiments were carried out under the same conditions using the related materials as the catalysts instead of **1-Sb_8Mo_{18}**. As shown in Table S10, the vastly different conversions of 100%, 74%, and 16% for **1-Sb_8Mo_{18}**, **2-$SiMo_{12}Sb_2$**, and **3-Mo_8** indicate that the strong Lewis basic sites Sb^{III} in POM play an important role for accelerating the reduction reaction, which is consistent with the previous reports.[29] $K_4[\beta\text{-}Mo_8O_{26}]$, [EMIm]Br, the equal proportion mixture of $K_4[\beta\text{-}Mo_8O_{26}]$ and [EMIm]Br, and **3-Mo_8** exhibited catalytic activities with conversions of 8%, 1%, 18%, and 16%, respectively. The catalysts containing both $[EMIm]^+$ cations and $[\beta\text{-}Mo_8O_{26}]^{4-}$ anions showed better activity. With the above results, we propose that the good catalytic activity of **1-Sb_8Mo_{18}** should be mainly attributed to the higher numbers of Sb^{III} sites and their synergistic effect with $[EMIm]^+$ cations.

Sustainability is a vital indicator of heterogeneous catalysts. As shown in Figure S16, almost no decrease was detected for the catalytic activity of **1-Sb_8Mo_{18}** after six cycles. Also, powder X-ray diffraction (PXRD), scanning electron microscopy (SEM), and energy-dispersive X-ray spectroscopy (EDX) for the fresh (POM isolated from the IL) and used samples were measured to investigate the stability of **1-Sb_8Mo_{18}**. For PXRD, the main diffraction peaks of the used sample are all well matched with those of the fresh one (Figure S17). In their SEM images (Figure S18), the used **1-Sb_8Mo_{18}** presents the same morphology of the micronanoblock as that of the ground fresh one. More importantly, the EDX data give the same ratio of Sb/Mo for the fresh and used samples (Table S13). All of the evidence above suggest that **1-Sb_8Mo_{18}** could keep its integrality during the recycling experiment.

In summary, the first member of a hexanuclear sandwich-type POMo compound (**1-Sb_8Mo_{18}**) containing the largest antimonomolybdate monomer with a Sb/Mo ratio of 8:18 has been directly synthesized by an ionothermal method and structurally characterized by single-crystal X-ray diffraction. More importantly, **1-Sb_8Mo_{18}** can be used as a sustainable catalyst with high activity to the reduction of nitroarenes. The kinetic study reveals that the reductions of the direct and indirect routes coexist simultaneously, while the former dominates the catalytic reaction process. In future work, we will explore more novel polynuclear clusters based on lacunary POMos with an ionothermal method as well as their catalytic behavior to the reduction of aromatic nitro compounds.

■ ASSOCIATED CONTENT

Supporting Information

The Supporting Information is available free of charge at https://pubs.acs.org/doi/10.1021/acs.inorgchem.0c00825.

Experimental details, crystallographic data and some other tables, and figures of characterizations and catalysis (PDF)

Accession Codes

CCDC 1978727, 1992938, and 1992939 contain the supplementary crystallographic data for this paper. These data can be obtained free of charge via www.ccdc.cam.ac.uk/data_request/cif, or by emailing data_request@ccdc.cam.ac.uk, or by contacting The Cambridge Crystallographic Data Centre, 12 Union Road, Cambridge CB2 1EZ, UK; fax: +44 1223 336033.

■ AUTHOR INFORMATION

Corresponding Authors

Dong-Bin Dang − *Henan Key Laboratory of Polyoxometalate Chemistry, College of Chemistry and Chemical Engineering, Henan University, Kaifeng, Henan 475004, P. R. China;* orcid.org/0000-0002-7042-2378; Email: dangdb@henu.edu.cn

Yan Bai − *Henan Key Laboratory of Polyoxometalate Chemistry, College of Chemistry and Chemical Engineering, Henan University, Kaifeng, Henan 475004, P. R. China;* Email: baiyan@henu.edu.cn

Authors

Shu-Kui Shi − *Henan Key Laboratory of Polyoxometalate Chemistry, College of Chemistry and Chemical Engineering, Henan University, Kaifeng, Henan 475004, P. R. China*

Xin Li − *Henan Key Laboratory of Polyoxometalate Chemistry, College of Chemistry and Chemical Engineering, Henan University, Kaifeng, Henan 475004, P. R. China; Engineering Technology Research Center of Henan Province for Solar Catalysis, College of Chemistry and Pharmaceutical Engineering, Nanyang Normal University, Nanyang, Henan 473061, P. R. China*

Hui-li Guo − *Henan Key Laboratory of Polyoxometalate Chemistry, College of Chemistry and Chemical Engineering, Henan University, Kaifeng, Henan 475004, P. R. China*

Yan-hua Fan − *Henan Key Laboratory of Polyoxometalate Chemistry, College of Chemistry and Chemical Engineering, Henan University, Kaifeng, Henan 475004, P. R. China*

Hai-yan Li − *Henan Key Laboratory of Polyoxometalate Chemistry, College of Chemistry and Chemical Engineering, Henan University, Kaifeng, Henan 475004, P. R. China*

Complete contact information is available at:
https://pubs.acs.org/10.1021/acs.inorgchem.0c00825

Notes

The authors declare no competing financial interest.

■ ACKNOWLEDGMENTS

This work was supported by the National Natural Science Foundation of China (Grant 21971055) and the Postdoctoral Scientific Fund of Henan Province (in 2019, third aid).

■ REFERENCES

(1) Gumerova, N. I.; Rompel, A. Synthesis, structures and applications of electron-rich polyoxometalates. *Nat. Rev. Chem.* **2018**, *2*, 1−12.

(2) Hampson, E.; Cameron, J.; Amin, S.; Kyo, J.; Watts, J.; Oshio, H.; Newton, G. N. Asymmetric hybrid polyoxometalates: a new platform for multifunctional redox-active nanomaterials. *Angew. Chem., Int. Ed.* **2019**, *58*, 18281−18285.

(3) Misra, A.; Kozma, K.; Streb, C.; Nyman, M. Beyond Charge Balance: Counter-Cations in Polyoxometalate Chemistry. *Angew. Chem., Int. Ed.* **2020**, *59*, 596−612.

(4) Chen, L.; Chen, W. L.; Wang, X. L.; Li, Y. G.; Su, Z. M.; Wang, E. B. Polyoxometalates in dye-sensitized solar cells. *Chem. Soc. Rev.* **2019**, *48*, 260−284.

(5) Tsubaki, S.; Hayakawa, S.; Ueda, T.; Fujii, S.; Suzuki, E. I.; Zhang, J.; Bond, A.; Wada, Y. Radio frequency alternating electromagnetic field enhanced tetraruthenium polyoxometalate electrocatalytic water oxidation. *Chem. Commun.* **2019**, *55*, 1032−1035.

(6) Bijelic, A.; Aureliano, M.; Rompel, A. Polyoxometalates as potential next-generation metallodrugs in the combat against cancer. *Angew. Chem., Int. Ed.* **2019**, *58*, 2980−2999.

(7) Samaniyan, M.; Mirzaei, M.; Khajavian, R.; Eshtiagh-Hosseini, H.; Streb, C. Heterogeneous catalysis by polyoxometalates in metal−organic frameworks. *ACS Catal.* **2019**, *9*, 10174−10191.

(8) Anyushin, A. V.; Kondinski, A.; Parac-Vogt, T. N. Hybrid polyoxometalates as post-functionalization platforms: from fundamentals to emerging applications. *Chem. Soc. Rev.* **2020**, *49*, 382−432.

(9) Yonesato, K.; Ito, H.; Itakura, H.; Yokogawa, D.; Kikuchi, T.; Mizuno, N.; Yamaguchi, K.; Suzuki, K. Controlled Assembly Synthesis of Atomically Precise Ultrastable Silver Nanoclusters with Polyoxometalates. *J. Am. Chem. Soc.* **2019**, *141*, 19550−19554.

(10) Li, Z.; Lin, L. D.; Yu, H.; Li, X. X.; Zheng, S. T. All-Inorganic Ionic Porous Material Based on Giant Spherical Polyoxometalates Containing Core-Shell K_6@ K_{36}-Water Cage. *Angew. Chem.* **2018**, *130*, 16003−16007.

(11) Combs-Walker, L. A.; Hill, C. L. Stabilization of the defect ("lacunary") complex polymolybdophosphate, $PMo_{11}O_{39}^{7-}$. Isolation, purification, stability characteristics, and metalation chemistry. *Inorg. Chem.* **1991**, *30*, 4016−4026.

(12) Li, S.; Zhao, J.; Ma, P.; Du, J.; Niu, J.; Wang, J. Rare sandwich-type polyoxomolybdates constructed from di-/tetra-nuclear transition-metal clusters and trivacant Keggin germanomolybdate fragments. *Inorg. Chem.* **2009**, *48*, 9819−9830.

(13) Zhang, Y. N.; Zhou, B. B.; Li, Y. G.; Su, Z. H.; Zhao, Z. F. A new molybdenum (V) nickel phosphate based on divacant $[H_{30}(Mo^{V}_{16}O_{32})Ni_{14}(PO_4)_{26}O_2(OH)_4(H_2O)_8]^{12-}$ wheel. *Dalton. Trans.* **2009**, *43*, 9446−9451.

(14) Li, C.; Mizuno, N.; Yamaguchi, K.; Suzuki, K. Self-Assembly of Anionic Polyoxometalate-Organic Architectures Based on Lacunary Phosphomolybdates and Pyridyl Ligands. *J. Am. Chem. Soc.* **2019**, *141*, 7687−7692.

(15) Bedrov, D.; Piquemal, J. P.; Borodin, O.; MacKerell, A. D., Jr; Roux, B.; Schröder, C. Molecular dynamics simulations of ionic liquids and electrolytes using polarizable force fields. *Chem. Rev.* **2019**, *119*, 7940−7995.

(16) Marinkovic, J. M.; Riisager, A.; Franke, R.; Wasserscheid, P.; Haumann, M. Fifteen years of supported ionic liquid phase-catalyzed hydroformylation: Material and process developments. *Ind. Eng. Chem. Res.* **2019**, *58*, 2409−2420.

(17) Rogers, R. D.; Seddon, K. R. Ionic liquids-solvents of the future? *Science* **2003**, *302*, 792−793.

(18) Seddon, K. R. Ionic liquids: a taste of the future. *Nat. Mater.* **2003**, *2*, 363.

(19) Santner, S.; Heine, J.; Dehnen, S. Synthesis of crystalline chalcogenides in ionic liquids. *Angew. Chem., Int. Ed.* **2016**, *55*, 876−893.

(20) Cooper, E. R.; Andrews, C. D.; Wheatley, P. S.; Webb, P. B.; Wormald, P.; Morris, R. E. Ionic liquids and eutectic mixtures as solvent and template in synthesis of zeolite analogues. *Nature* **2004**, *430*, 1012.

(21) Freudenmann, D.; Wolf, S.; Wolff, M.; Feldmann, C. Ionic liquids: new perspectives for inorganic synthesis? *Angew. Chem., Int. Ed.* **2011**, *50*, 11050−11060.

(22) Lin, S.; Liu, W.; Li, Y.; Wu, Q.; Wang, E.; Zhang, Z. Preparation of polyoxometalates in ionic liquids by ionothermal synthesis. *Dalton. Trans.* **2010**, *39*, 1740−1744.

(23) Jiang, Z. G.; Shi, K.; Lin, Y. M.; Wang, Q. M. $[Ag_{70}(PW_9O_{34})_2(^{t}BuC{\equiv}C)_{44}(H_2O)_2]^{8+}$: ionothermal synthesis of a silver cluster encapsulating lacunary polyoxometalate ions. *Chem. Commun.* **2014**, *50*, 2353−2355.

(24) Aidoudi, F. H.; Aldous, D. W.; Goff, R. J.; Slawin, A. M.; Attfield, J. P.; Morris, R. E.; Lightfoot, P. An ionothermally prepared S= 1/2 vanadium oxyfluoride kagome lattice. *Nat. Chem.* **2011**, *3*, 801.

(25) Sokolov, M. N.; Izarova, N. V.; Virovets, A. V.; Fedin, V. P.; Starikova, Z. A.; Antipin, M. Y. Preparation and structure of $[Sn_8W_{18}O_{66}]^{8-}$ - a 26-nuclear stannotungstate with a hexagonal belt of six Sn(II) ions with outward-looking lone pairs. *Dalton. Trans.* **2003**, *23*, 4389.

(26) Zhao, H.; Tao, L.; Zhang, F.; Zhang, Y.; Liu, Y.; Xu, H.; Diao, G.; Ni, L. Transition metal substituted sandwich-type polyoxometalates with a strong metal-C (imidazole) bond as anticancer agents. *Chem. Commun.* **2019**, *55*, 1096−1099.

(27) Wang, Y. J.; Wu, S. Y.; Sun, Y. Q.; Li, X. X.; Zheng, S. T. Octahedron-shaped three-shell Ln_{14}-substituted polyoxotungstogermanates encapsulating a W_4O_{15} cluster: luminescence and frequency dependent magnetic properties. *Chem. Commun.* **2019**, *55*, 2857−2860.

(28) Wang, Y.; Lu, J.; Ma, X.; Niu, Y.; Singh, V.; Ma, P.; Zhang, C.; Niu, J.; Wang, J. Synthesis, characterization and catalytic oxidation of organosilanes with a novel multilayer polyoxomolybdate containing mixed-valence antimony. *Mol. Catal.* **2018**, *452*, 167−174.

(29) Yu, F.; Xu, L. Highly efficient $Mo^{IV}_3\cdots Sb^{III}$ cluster frustrated Lewis pair hydrogenation. *Dalton. Trans.* **2019**, *48*, 17445−17450.

(30) Wang, W. W.; Lv, J. H.; Yu, K.; Wang, C. M.; Zhang, H.; Wu, C.; Zhou, B. B. The basket-type dimer layers based on tetra-electron reduced heteropoly blue directed by copper/nickel and strontium linkers. *New J. Chem.* **2017**, *41*, 2687−2694.

(31) Zhang, Z. X.; Sadakane, M.; Murayama, T.; Izumi, S.; Yasuda, N.; Sakaguchi, N.; Ueda, W. Tetrahedral connection of ε-keggin-type polyoxometalates to form an all-inorganic octahedral molecular sieve with an intrinsic 3D pore system. *Inorg. Chem.* **2014**, *53*, 903−911.

(32) Bagherjeri, F. A.; Vonci, M.; Nagul, E. A.; Ritchie, C.; Gable, R. W.; Taylor, M. B.; Bryant, G.; Guo, S.-X.; Zhang, J.; Aparicio, P. A.; Lopez, X.; Poblet, J. M.; Boskovic, C. Mixed-Metal Hybrid Polyoxometalates with Amino Acid Ligands: Electronic Versatility and Solution Properties. *Inorg. Chem.* **2016**, *55*, 12329−12347.

(33) Assran, A. S.; Izarova, N. V.; Banerjee, A.; Rabie, U. M.; Abou-El-Wafa, M. H. M.; Kortz, U. The antimony(III)-bridged heteropolyanion sandwich dimers $[Sb^{III}_3(A\text{-}\alpha\text{-}XW_9O_{34})_2]^{11-}$ (X = Si^{IV}, Ge^{IV}) and C-shaped double-sandwich $[Sb^{III}_6O_2(PW_6O_{26})(A\text{-}\alpha\text{-}PW_9O_{34})_2]^{15-}$. *Dalton Trans.* **2012**, *41*, 9914−9921.

(34) Brown, I. D.; Altermatt, D. Bond-Valence Parameters Obtained from a Systematic Analysis of the Inorganic Crystal Structure Database. *Acta Crystallogr., Sect. B: Struct. Sci.* **1985**, *41*, 244−247.

(35) Calin, N.; Sevov, S. C. Novel Mixed-Valence Heteropolyoxometalates: A Molybdenum Diphosphonate Anion $[Mo^{V}{}_7Mo^{VI}O_{16}(O_3PPhPO_3H)_4]^{3-}$ and Its One-and Two-Dimensional Assemblies. *Inorg. Chem.* **2003**, *42*, 7304−7308.

(36) Tan, S.; Hobday, M.; Gorman, J.; Amiet, G.; Rix, C. Preparation and characterisation of some new Mo/O/XR (X= P or As) heteropoly blue complexes. *J. Mater. Chem.* **2003**, *13*, 1180−1185.

(37) Zhang, X. M.; Wu, H. S.; Zhang, F. Q.; Prikhod'ko, A.; Kuwata, S.; Comba, P. The three-electron heteropoly blue $[P_6Mo_{18}O_{73}]^{11-}$ with a basket-shaped skeleton. *Chem. Commun.* **2004**, *18*, 2046−2047.

(38) Sassoye, C.; Norton, K.; Sevov, S. C. $[Mo_5{}^{V}Mo_7{}^{VI}O_{30}(BPO_4)_2(O_3P\text{-}Ph)_6]^{5-}$: A Phenyl-Substituted Molybdenum (V/VI) Boro-Phosphate Polyoxometalate. *Inorg. Chem.* **2003**, *42*, 1652−1655.

(39) Dumas, E.; Debiemme-Chouvy, C.; Sevov, S. C. A Reduced PolyoxomolybdenumBorophosphate Anion Related to the Wells−Dawson Clusters. *J. Am. Chem. Soc.* **2002**, *124*, 908−909.

(40) Song, J. j.; Huang, Z. F.; Pan, L.; Li, K.; Zhang, X. G.; Wang, L.; Zou, J. J. Review on selective hydrogenation of nitroarene by catalytic, photocatalytic and electrocatalytic reactions. *Appl. Catal., B* **2018**, *227*, 386−408.

(41) Hu, H. W.; Xin, J. H.; Hu, H.; Wang, X. W.; Miao, D. G.; Liu, Y. Synthesis and stabilization of metal nanocatalysts for reduction reactions − a review. *J. Mater. Chem. A* **2015**, *3*, 11157.

(42) Kadam, H. K.; Tilve, S. G. Advancement in methodologies for reduction of nitroarenes. *RSC Adv.* **2015**, *5*, 83391.

(43) Orlandi, M.; Brenna, D.; Harms, R.; Jost, S.; Benaglia, M. Recent Developments in the Reduction of Aromatic and Aliphatic Nitro Compounds to Amines. *Org. Process Res. Dev.* **2018**, *22*, 430−445.

(44) Papadas, I. T.; Fountoulaki, S.; Lykakis, I. N.; Armatas, G. S. Controllable synthesis of mesoporous iron oxide nanoparticle assemblies for chemoselective catalytic reduction of nitroarenes. *Chem. - Eur. J.* **2016**, *22*, 4600−4607.

(45) Formenti, D.; Ferretti, F.; Scharnagl, F. K.; Beller, M. Reduction of Nitro Compounds Using 3d-Non-Noble Metal Catalysts. *Chem. Rev.* **2019**, *119*, 2611−2680.

(46) Schomberg, F.; Zi, Y.; Vilotijevic, I. Lewis-base-catalysed selective reductions of ynones with a mild hydride donor. *Chem. Commun.* **2018**, *54*, 3266−3269.

(47) Radai, Z.; Kiss, N. Z.; Keglevich, G. An overview of the applications of ionic liquids as catalysts and additives in organic chemical reactions. *Curr. Org. Chem.* **2018**, *22*, 533−556.

(48) Luo, B.; Sang, R.; Lin, L.; Xu, L. $Mo^{IV}{}_3$-Polyoxomolybdates with frustrated Lewis pairs for high-performance hydrogenation catalysis. *Catal. Sci. Technol.* **2019**, *9*, 65−69.

(49) Luo, B.; Xu, L. POM-FLPs:$[Mo^{IV}{}_3]_n$-polyoxometalatebifunctional catalysis by $[Mo^{IV}{}_3]_n\text{-}O_m$ Lewis pairs frustrated by triangular $Mo^{IV}\text{-}Mo^{IV}$ bonds. *Dalton.Trans.* **2019**, *48*, 6892−6898.

(50) Lara, P.; Philippot, K. The hydrogenation of nitroarenes mediated by platinum nanoparticles: An overview. *Catal. Sci. Technol.* **2014**, *4*, 2445−2465.

(51) Sheng, Y.; Wang, X.; Xing, Z.; Chen, X.; Zou, X.; Lu, X. Highly Active and Chemoselective Reduction of Halogenated Nitroarenes Catalyzed by Ordered Mesoporous Carbon Supported Platinum Nanoparticles. *ACS Sustainable Chem. Eng.* **2019**, *7*, 8908−8916.

(52) Kadam, H. K.; Tilve, S. G. Advancement in methodologies for reduction of nitroarenes. *RSC Adv.* **2015**, *5*, 83391−83407.

(53) Zhang, C. F.; Zhang, Z. X.; Wang, X.; Li, M. R.; Lu, J. M.; Si, R.; Wang, F. *Appl. Catal., A* **2016**, *525*, 85−93.

(54) Zhang, C. F.; Wang, X.; Li, M. R.; Zhang, Z. X.; Wang, Y. H.; Si, R.; Wang, F. A switchable-selectivity multiple-interface Ni-WC hybrid catalyst for efficient nitroarene reduction. *Chin. J. Catal.* **2016**, *37*, 1569−1577.